Parameter Variations of Equivalent Circuit Model of Lithium-ion Capacitor

Mohammad K. Al-Smadi, *Student Member*, *IEEE* and Jaber A. Abu Qahouq, *Senior Member*, *IEEE*

The University of Alabama
Department of Electrical and Computer Engineering
Tuscaloosa, Alabama 35487, USA

***Abstract*— This paper presents characterization for equivalent circuit model (ECM) parameters variation for lithium-ion capacitor (LiC) under different voltage values. A set of experimentally obtained electrochemical impedance spectroscopy (EIS) data for LiC is fitted using the simplex algorithm to obtain the values for ECM parameters. The model-fit EIS data is compared with the measured EIS data to validate the model.**

Keywords—Energy storage, lithium-ion capacitor, hybrid capacitor, electrochemical impedance spectroscopy (EIS), impedance, equivalent circuit model (ECM), capacitance.

I. INTRODUCTION

Energy storage devices are needed in a wide range of applications such as electric vehicles, uninterruptible power supplies (UPS), and renewable energy systems [1-13]. Energy storage devices are mainly characterized by their energy density power density, cost, and their ability to withstand fast charge and discharge [14, 15]. Lithium-ion batteries (LiB) are commonly used for applications that require high energy density (i.e., long-term energy storage). However, their power density and lifecycle can, sometimes, hinder their performance in applications where high power/current is needed. Supercapacitors (SC) have a higher power density compared to LiB, but much lower energy density. Therefore, SC can serve as a short-term energy storage and is well-suited for applications requiring a high power/current for a short time. Lithium-ion capacitors (LiC) combine high energy density from LiB with high power density from SC [16-18]. In the literature, various applications are reported for LiC such as electric vehicles [17, 18], renewable energy and grid [16, 19], and railway transportation [20].

Electrochemical impedance spectroscopy (EIS) is usually utilized to gain insights on the internal mechanisms and dynamics of energy storage devices. EIS data can be utilized to perform diagnosis and state estimation (state of charge "SOC" and state of health "SOH") [21-23]. EIS measurements are usually performed in potentiostatic mode or galvanostatic mode. In potentiostatic mode, an AC voltage perturbation $v_{ac\text{-}fp}$ with a perturbation frequency f_p is applied to the device under test (LiC in this paper) and the AC current response $i_{ac\text{-}fp}$ is recorded. In galvanostatic mode, the device under test is excited by an AC current perturbation where the AC voltage response is recorded. In both modes, the impedance is calculated as expressed in (1).

$$Z_{fp} = \frac{v_{ac-f_p}}{i_{ac-f_p}} e^{j\theta_{z-fp}} \quad (1)$$

Table I- Equivalent circuit model parameters [24]

ECM model component	Description	Frequency range
R_{Cond}	Electrolyte resistance	Medium
R_{HF}	Metal connections	High
L_{HF}		
R_{CT1}	Charge transfer	Low to medium
C_{CT1}		
R_{CT2}		
C_{CT2}		
W	Diffusion	Low
R_D		

where Z_{fp} is the impedance at the perturbation frequency f_p, $v_{ac\text{-}fp}$ is the peak (amplitude) voltage value at the fundamental perturbation frequency f_p, and $i_{ac\text{-}fp}$ is the peak (amplitude) current value at the fundamental perturbation frequency f_p. The impedance phase is represented by $\theta_{z\text{-}fp}$ and is equal to the phase shift between the fundamental components of voltage and current of the device under test, i.e., $\theta_{z\text{-}fp} = \theta_{v\text{-}fp} - \theta_{i\text{-}fp}$. In potentiostatic mode, $v_{ac\text{-}fp}$ is applied and $i_{ac\text{-}fp}$ is recorded where in galvanostatic mode $i_{ac\text{-}fp}$ is applied and $v_{ac\text{-}fp}$ is recorded. To obtain a spectrum of EIS data across a range of frequencies, the device under test is perturbed at different frequencies and the impedance value (both magnitude and phase) is calculated at each frequency.

To fit the measured EIS data, electrical circuit model (ECM) is utilized. ECM allows for internal dynamics characterization of various energy storage devices. In this paper, an experimentally-obtained EIS data for LiC is utilized to obtain the ECM parameters at different voltage values. The obtained ECM parameters can be used in state estimation of LiC or in other functions.

II. ECM FOR LITHIUM-ION CAPACITOR

Fig. 1 shows the LiC ECM [24] considered in this paper to fit the EIS data in order to obtain and characterize parameter variation patterns of LiC under different voltage values. The explanation for each ECM parameter is illustrated in Table I. The inductive part L_{HF} and the resistive part R_{HF} are used to model the cable and connections effect at high frequency. The electrolyte resistance is represented by R_{Cond} while the

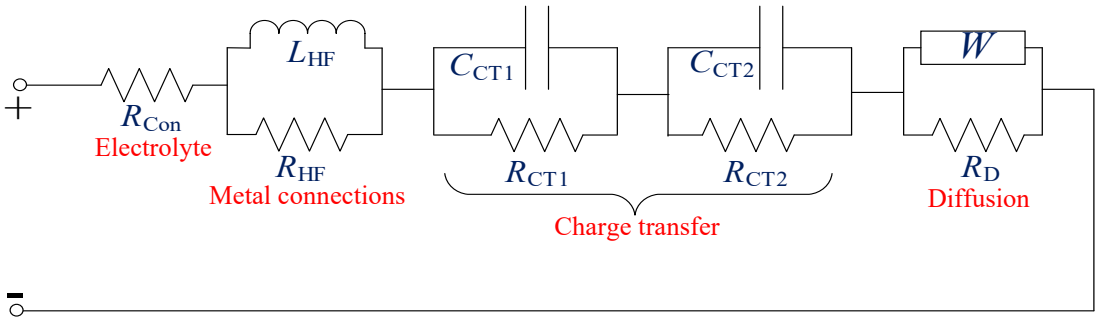

Fig. 1: Equivalent circuit model for LiC [24].

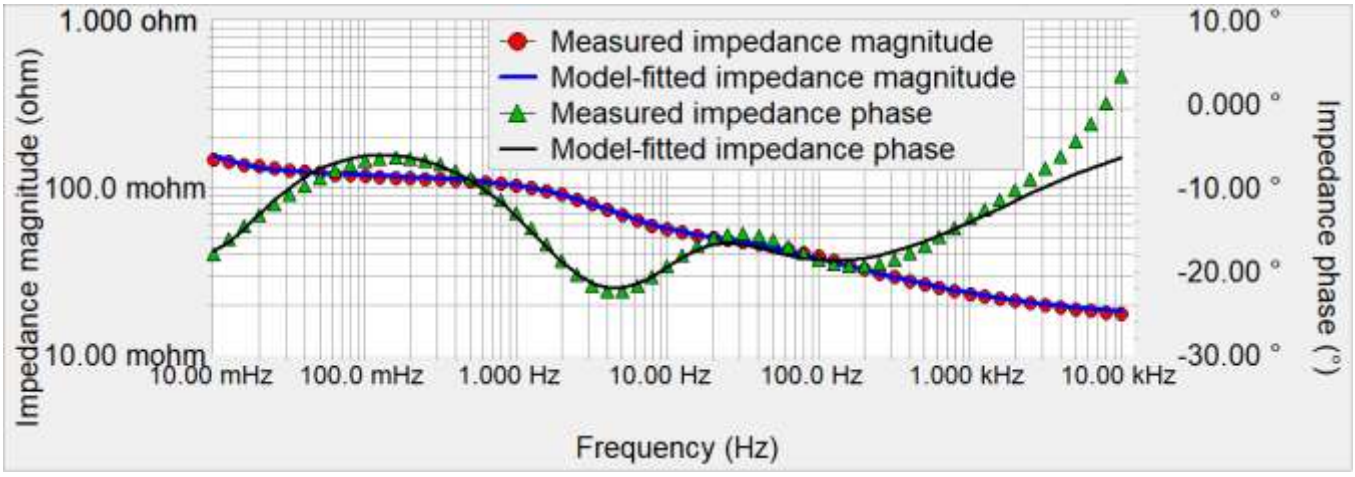

(a)

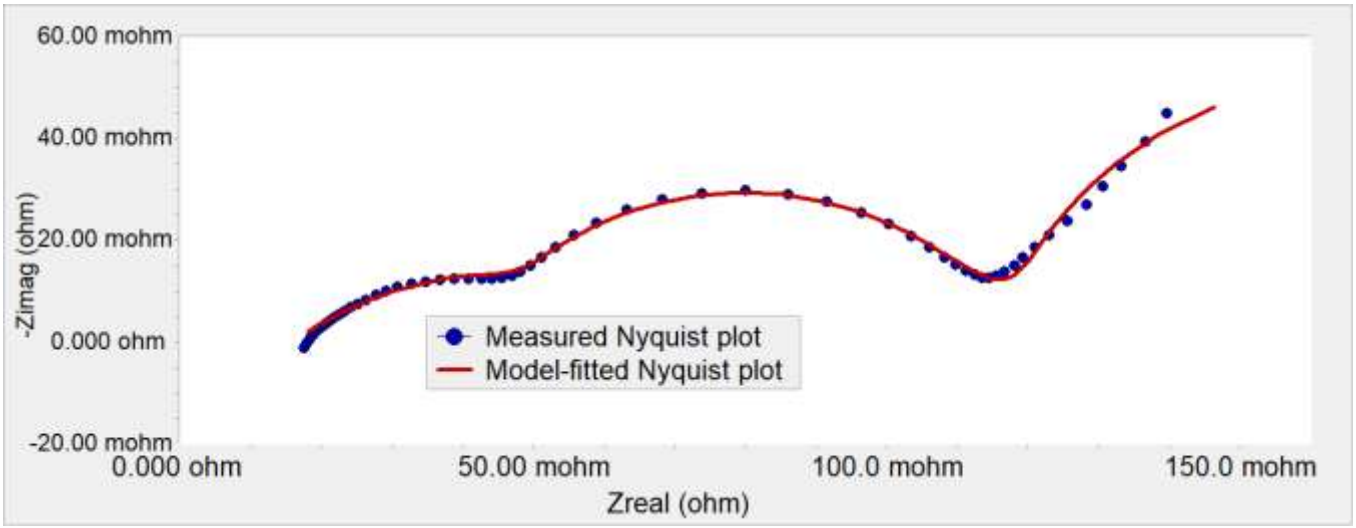

(b)

Fig. 2: Comparison between measured EIS and equivalent circuit model-fitted EIS data. (a) Impedance magnitude and phase. (b) Nyquist plot.

chargetransfer process or polarization is represented by two RC parallel branches (R_{CT1} with C_{CT1} and R_{CT2} with C_{CT2}). The capacitances C_{CT1} and C_{CT2} represent the electrode's double-layer capacitance, where R_{CT1} and R_{CT2} represent the charge transfer resistance. Warburg impedance W and its parallel resistance R_D are used to model ions diffusion. Since ions diffusion is a slow process, the low frequency impedance in the EIS curve is mainly dominated by W and R_D.

The EIS data is obtained using Gamry Instruments Interface 5000E™ [25]. Gamry Echem analyst software [26] is utilized in this paper to fit the measured EIS data using the simplex algorithm, which is used to solve linear programming problems [27].

Fig. 2 shows a comparison between the measured EIS plots at 3.0V and the fitted plots using the simplex algorithm. In

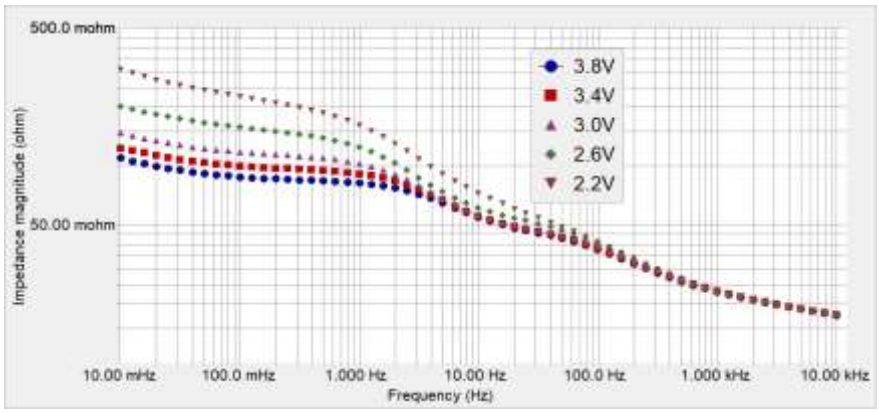

(a)

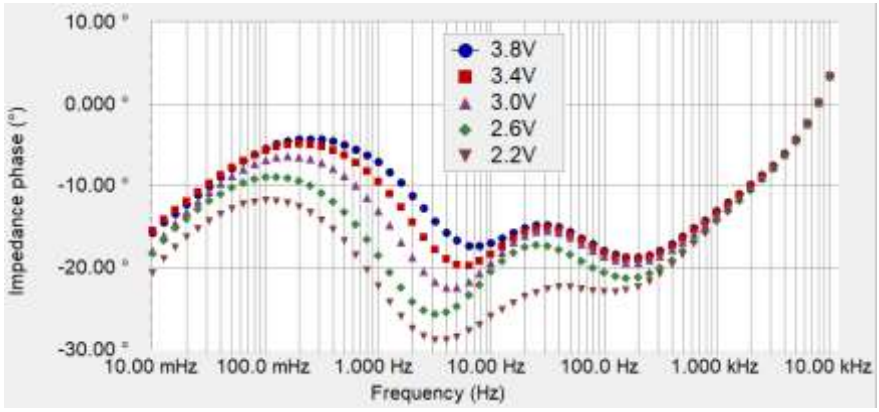

(b)

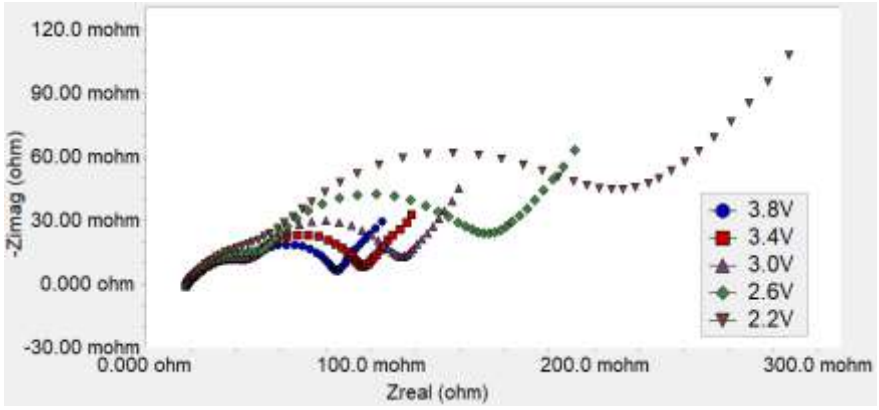

(c)

Fig. 3: Impedance plots for LiC at different voltage values. (a) Impedance magnitude. (b) Impedance phase. (c) Nyquist plot.

Fig. 2(a), the impedance magnitude and phase plots are compared, where in Fig. 2(b), the Nyquist plots are compared. As illustrated, the fitted plots are in good agreement with the measured plots, which allows for using the ECM of Fig. 1 to fit the obtained EIS curves to the ECM parameters.

III. Experimental Results

In this paper, a 450F LiC [28] is used. The EIS measurements are obtained by performing galvanostatic EIS at different voltage values including 3.8V (maximum voltage), 3.4V, 3.0V, 2.6V, and 2.2V (minimum voltage), within a frequency range of 10kHz to 0.01Hz at room temperature (~25ºC). EIS plots at different voltage values are shown in Fig. 3. As shown in Fig. 3 (a), the LiC impedance magnitude increases as the voltage of the LiC decreases, especially at low frequency. This is because at lower voltage values, the anode energy is low which makes the diffusion process slow [24]. Also, by looking at the high frequency range (above ~1kHz) in both impedance magnitude and phase plots (Fig. 3a and Fig. 3b), it can be observed that the LiC impedance magnitude and phase do not change with voltage, and that is also clear from the matching Nyquist plots at different voltage values at high

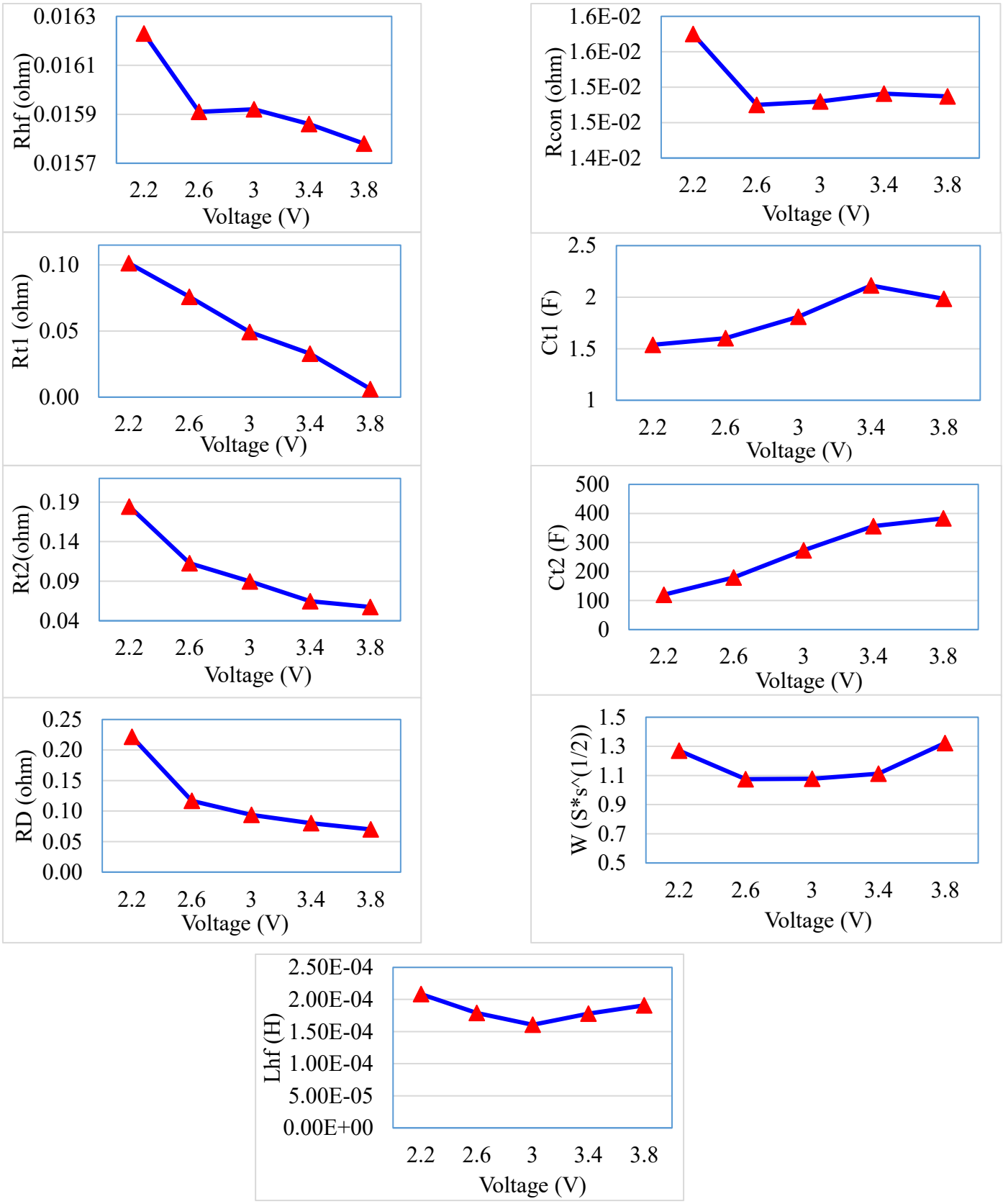

Fig. 4: ECM parameter variation of LiC at different voltage levels.

frequency (left part of the Nyquist plot as shown in Fig. 3c). From the Nyquist plot in Fig. 3 (c), it can be observed that the semi-circle radius increases as the LiC voltage decreases. The semi-circle represents the charge transfer process that occurs at medium frequency [24]. The lower is the voltage of the LiC, the higher is the charge transfer resistance. The right part of the Nyquist plot (almost a straight line with a slope of ~45º) is associated with the diffusion process (i.e., Warburg impedance)

The obtained EIS curves are utilized to fit the ECM parameters. The variation of each parameter is shown in Fig. 4. As illustrated, the charge transfer capacitance increases at high voltage values. Also, the charge transfer resistance increases at low voltage values. As mentioned earlier, lower voltage results in slower diffusion process which implies a higher charge transfer resistance.

IV. Conclusion

In this paper, ECM parameter variation for LiC is characterized by fitting the measured EIS data at different voltage values using the simplex algorithm. The EIS data was collected under galvanostatic mode. The model-fitted data is compared with the measured EIS data to validate the model fitting.

Acknowledgement

This material is based upon work supported in part by the National Science Foundation under Grant No. 2213918. Any opinions, findings and conclusions or recommendations expressed in this material are those of the author(s) and do not necessarily reflect the views of the National Science Foundation.

V. References

[1] M. Aamir, K. Ahmed Kalwar, and S. Mekhilef, "Review: Uninterruptible Power Supply (UPS) system," *Renewable and Sustainable Energy Reviews,* vol. 58, pp. 1395-1410, 05/01/ 2016.

[2] M. K. Al-Smadi and J. A. Abu Qahouq, "Hybrid Lithium Capacitor Voltage Balancing with Planar Power Inductor for Electric Vehicles and Other Applications," in *2023 IEEE Applied Power Electronics Conference and Exposition (APEC)*, 19-23 March 2023 2023, pp. 2845-2850, doi: 10.1109/APEC43580.2023.10131569.

[3] M. K. Al-Smadi and J. A. Abu Qahouq, "Evaluation of Current-Mode Controller for Active Battery Cells Balancing With Peak Efficiency Operation," *IEEE Transactions on Power Electronics,* vol. 38, no. 2, pp. 1610-1621, 2023, doi: 10.1109/TPEL.2022.3211905.

[4] Y. Cao and J. A. Abu Qahouq, "Hierarchical SOC Balancing Controller for Battery Energy Storage System," *IEEE Transactions on Industrial Electronics,* vol. 68, no. 10, pp. 9386-9397, 2021, doi: 10.1109/TIE.2020.3021608.

[5] W. Huang and J. A. Abu Qahouq, "Energy Sharing Control Scheme for State-of-Charge Balancing of Distributed Battery Energy Storage System," *IEEE Transactions on Industrial Electronics,* vol. 62, no. 5, pp. 2764-2776, 2015, doi: 10.1109/TIE.2014.2363817.

[6] S. D. G. Jayasinghe, D. M. Vilathgamuwa, and U. K. Madawala, "A dual inverter based supercapacitor direct integration scheme for wind energy conversion systems," in *2010 IEEE International Conference on Sustainable Energy Technologies (ICSET)*, 6-9 Dec. 2010 2010, pp. 1-6, doi: 10.1109/ICSET.2010.5684459.

[7] S. Kim, M. Kwon, and S. Choi, "Operation and Control Strategy of a New Hybrid ESS-UPS System," *IEEE Transactions on Power Electronics,* vol. 33, no. 6, pp. 4746-4755, 2018, doi: 10.1109/TPEL.2017.2733019.

[8] D. Linzen, S. Buller, E. Karden, and R. W. D. Doncker, "Analysis and evaluation of charge-balancing circuits on performance, reliability, and lifetime of supercapacitor systems," *IEEE Transactions on Industry Applications,* vol. 41, no. 5, pp. 1135-1141, 2005, doi: 10.1109/TIA.2005.853375.

[9] A. E. Mejdoubi, A. Oukaour, H. Chaoui, Y. Slamani, J. Sabor, and H. Gualous, "Online Supercapacitor Diagnosis for Electric Vehicle Applications," *IEEE Transactions on Vehicular Technology,* vol. 65, no. 6, pp. 4241-4252, 2016, doi: 10.1109/TVT.2015.2454520.

[10] S. Vonsien and R. Madlener, "Li-ion battery storage in private households with PV systems: Analyzing the economic impacts of battery aging and pooling," *Journal of Energy Storage,* vol. 29, p. 101407, 06/01/ 2020.

[11] Z. Xia and J. A. Abu Qahouq, "Ageing characterization data of lithium-ion battery with highly deteriorated state and wide range of state-of-health," *Data in Brief,* vol. 40, p. 107727, 02/01/ 2022.

[12] Z. Xia and J. A. Abu Qahouq, "Lithium-Ion Battery Ageing Behavior Pattern Characterization and State-of-Health Estimation Using Data-Driven Method," *IEEE Access,* vol. 9, pp. 98287-98304, 2021, doi: 10.1109/ACCESS.2021.3092743.

[13] Z. Yu, D. Zinger, and A. Bose, "An innovative optimal power allocation strategy for fuel cell, battery and supercapacitor hybrid electric vehicle," *Journal of Power Sources,* vol. 196, no. 4, pp. 2351-2359, 02/15/ 2011.

[14] R. de Fazio, D. Cafagna, G. Marcuccio, and P. Visconti, "Limitations and Characterization of Energy Storage Devices for Harvesting Applications," *Energies*, vol. 13, no. 4, doi: 10.3390/en13040783.

[15] W. Tasnin and L. C. Saikia, "Performance comparison of several energy storage devices in deregulated AGC of a multi-area system incorporating geothermal power plant," *IET Renewable Power Generation,* vol. 12, no. 7, pp. 761-772, 05/01 2018.

[16] S. A. Hamidi, E. Manla, and A. Nasiri, "Li-ion batteries and Li-ion ultracapacitors: Characteristics, modeling and grid applications," in *2015 IEEE Energy Conversion Congress and Exposition (ECCE)*, 20-24 Sept. 2015, pp. 4973-4979.

[17] N. Omar *et al.*, "Assessment of lithium-ion capacitor for using in battery electric vehicle and hybrid electric vehicle applications," *Electrochimica Acta,* vol. 86, pp. 305-315, 12/30/ 2012.

[18] M. Soltani *et al.*, "Hybrid Battery/Lithium-Ion Capacitor Energy Storage System for a Pure Electric Bus for an Urban Transportation Application," *Applied Sciences*, vol. 8, no. 7, doi: 10.3390/app8071176.

[19] K. Koyanagi *et al.*, "A Smart Photovoltaic Generation System Integrated with Lithium-ion Capacitor Storage," in *2011 46th International Universities' Power Engineering Conference (UPEC)*, 5-8 Sept. 2011 2011, pp. 1-6.

[20] F. Ciccarelli, A. D. Pizzo, and D. Iannuzzi, "Improvement of Energy Efficiency in Light Railway Vehicles Based on Power Management Control of Wayside Lithium-Ion Capacitor Storage," *IEEE Transactions on Power Electronics,* vol. 29, no. 1, pp. 275-286, 2014, doi: 10.1109/TPEL.2013.2253492.

[21] S. Rodrigues, N. Munichandraiah, and A. K. Shukla, "A review of state-of-charge indication of batteries by means of a.c. impedance measurements," *Journal of Power Sources,* vol. 87, no. 1, pp. 12-20, 04/01/ 2000.

[22] J. Segalini, B. Daffos, P. L. Taberna, Y. Gogotsi, and P. Simon, "Qualitative Electrochemical Impedance Spectroscopy study of ion transport into sub-nanometer carbon pores in Electrochemical Double Layer Capacitor electrodes," *Electrochimica Acta,* vol. 55, no. 25, pp. 7489-7494, 10/30/ 2010.

[23] U. Westerhoff, K. Kurbach, F. Lienesch, and M. Kurrat, "Analysis of Lithium-Ion Battery Models Based on Electrochemical Impedance Spectroscopy," *Energy Technology,* vol. 4, no. 12, pp. 1620-1630, 12/01 2016

[24] Y. Firouz, N. Omar, J. M. Timmermans, P. Van den Bossche, and J. Van Mierlo, "Lithium-ion capacitor – Characterization and development of new electrical model," *Energy,* vol. 83, pp. 597-613, 04/01/ 2015.

[25] Interface 5000E™ potentiostat, Gamry Instruments. [Online]. Available: https://www.gamry.com/potentiostats/interface-5000epotentiostat/.

[26] Gamry Echem Analyst software. [Online]. Aailable: https://www.gamry.com/assets/Support-Downloads/Quick-Start-Guides/EchemAnalystSoftwareManual.pdf

[27] Y.-S. Kim, "Refined simplex method for data fitting," in *Astronomical Data Analysis Software and Systems VI*, 1997, vol. 125, p. 206.

[28] Tecate 450 F (EDLC) Supercapacitor, 2022. Accessed: Aug. 19, 2022. [Online].Available:https://www.tecategroup.com/products/data_sheet.php?t=SERIES&i=TPLC